



HAL
open science

VISCOSITY MEASUREMENTS IN THE NEMATIC AND SMECTIC A PHASES OF A LIQUID CRYSTAL CRITICAL BEHAVIOUR

L. Léger, A. Martinet

► **To cite this version:**

L. Léger, A. Martinet. VISCOSITY MEASUREMENTS IN THE NEMATIC AND SMECTIC A PHASES OF A LIQUID CRYSTAL CRITICAL BEHAVIOUR. *Journal de Physique Colloques*, 1976, 37 (C3), pp.C3-89-C3-97. 10.1051/jphyscol:1976316 . jpa-00216499

HAL Id: jpa-00216499

<https://hal.science/jpa-00216499>

Submitted on 4 Feb 2008

HAL is a multi-disciplinary open access archive for the deposit and dissemination of scientific research documents, whether they are published or not. The documents may come from teaching and research institutions in France or abroad, or from public or private research centers.

L'archive ouverte pluridisciplinaire **HAL**, est destinée au dépôt et à la diffusion de documents scientifiques de niveau recherche, publiés ou non, émanant des établissements d'enseignement et de recherche français ou étrangers, des laboratoires publics ou privés.

VISCOSITY MEASUREMENTS IN THE NEMATIC AND SMECTIC A PHASES OF A LIQUID CRYSTAL CRITICAL BEHAVIOUR

L. LÉGER and A. MARTINET

Laboratoire de Physique des Solides, Université Paris-Sud, 91405 Orsay, France

Résumé. — Les trois viscosités η_1, η_3, η_2 correspondant respectivement à une orientation planaire avec le directeur parallèle ou perpendiculaire à la vitesse ou homéotrope, ont été mesurées dans du 4-n-octyloxy-4-cyanobiphényle pour un écoulement de Poiseuille dans un canal à section rectangulaire. Dans la phase nématique, η_1 montre une forte divergence près de la température de transition nématique/smectique, T_{NA} , compatible avec un exposant critique $\nu = 0,36 \pm 0,05$ sur trois décades de température, tandis que η_2 et η_3 ont un comportement régulier. La viscosité de torsion γ_1 et la tension superficielle ont également été mesurées. La divergence de γ_1 est compatible avec celle trouvée pour η_1 . Dans la phase smectique, on observe un régime de perméation quand l'écoulement se fait perpendiculairement aux plans smectiques et on a alors une énorme anisotropie de viscosité ($\eta_1/\eta_2 \simeq 150$ pour $\Delta T \simeq 3 \times 10^{-1}$ °C).

Abstract. — Measurements in a rectangular channel of the three viscosities η_1, η_3, η_2 for laminar flow with the director parallel or perpendicular to the velocity or homeotropic orientation respectively, are reported for 4-n-octyloxy-4-cyanobiphenyl. In the nematic range, η_1 has a pronounced divergence near the nematic/smectic transition temperature T_{NA} compatible with a critical exponent $\nu = 0.36 \pm 0.05$, over three decades of temperature, while η_2 and η_3 remain regular. The twist viscosity γ_1 and the surface tension have also been measured. The divergence of γ_1 is compatible with that of η_1 . In the smectic range, a permeation regime is observed when the flow is normal to the smectic layers leading to a very large anisotropy of the viscosities ($\eta_1/\eta_2 \simeq 150$ for $\Delta T \simeq 3 \times 10^{-1}$ °C).

1. Introduction. — There has been a considerable interest recently in describing accurately the critical behaviour of the static and dynamic properties of a nematic near a second order nematic to smectic A phase transition.

From a theoretical point of view, two kinds of approach have been developed: the McMillan school which, in the frame of a Landau approximation, predicts a coherence length ξ varying as $(T - T_c)^{-1/2}$, and a renormalization of bend, twist elastic constants and of some viscosities proportional to ξ [1] — the de Gennes' school, which, from an analogy with the λ transition of helium, predicts $\xi \sim (T - T_c)^{-2/3}$, bend and twist elastic constants proportional to ξ [2], and a renormalization of some viscosities proportional to $\xi^{1/2}$ [3, 4]. More recently, it has been pointed out that, because of the strong coupling between the nematic director and the smectic order parameter, the transition should always be at least weakly first order [5], but if the first order character of the transition is sufficiently weak, we can still expect the behaviour of a second order one, with an extrapolated transition temperature T^* smaller than T_c .

Experimentally, a wide variety of exponents have been found, especially in the case of the twist viscosity γ_1 for which values as different as 0.33 and 1 have been

reported [6, 7]. Such discrepancies are certainly due to the fact that most of those results have been obtained by working relatively far from T_c ($\Delta T \gtrsim 10^{-1}$ °C). The critical exponents are then very sensitive to the unknown non divergent γ_1 contribution. One measurement [8], from light scattering, has been made much closer to T_c ($\Delta T \sim 10^{-3}$ °C), but the relaxation time of the orientational fluctuations is proportional to γ_1/K_2 , and one needs an independent measurement of the divergent twist elastic constant K_2 to deduce γ_1 .

γ_1 has been the most widely studied viscosity coefficient but some others are also predicted to diverge at the nematic-smectic A transition. A rather convenient one seems to be the viscosity η_1 (Fig. 1) corresponding to a flow velocity parallel to the molecules. It is expected to diverge in the same way as γ_1 [3, 4] ($\delta\eta_1 = \delta\gamma_1$ where $\delta\eta_1$ and $\delta\gamma_1$ denote the pretransitional contribution to η_1 and γ_1), and one can hope that the background term would be less important than in the case of γ_1 (η_1 is the smallest viscosity in usual nematics).

In this paper, we present measurements of η_1, η_2, η_3 in the whole nematic range of 4-cyano-4'-n-octyloxy-biphenyl. η_1 diverges close to the nematic smectic A transition ($\Delta T \gtrsim 10^{-2}$ °C), while the two other viscosities η_2 and η_3 (molecules normal to the flow and respectively parallel or normal to the velocity gradient),

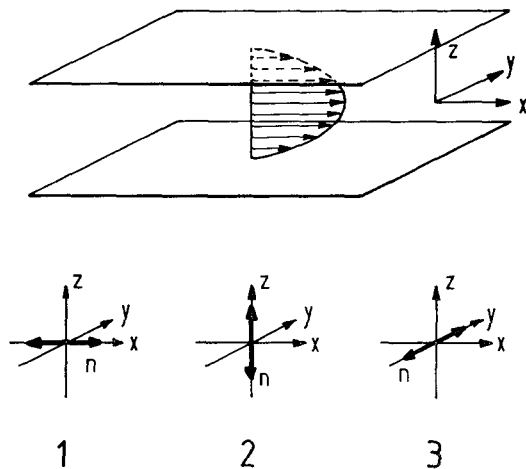


FIG. 1. — Sketch of the flow in the channel with the three different geometries corresponding respectively to η_1 (director parallel to the velocity), η_2 (director perpendicular to the velocity and parallel to the velocity gradient), η_3 (director perpendicular to the velocity and to the velocity gradient).

(Fig. 1) remain regular as predicted. For comparison, the temperature dependence of γ_1 has also been measured in the same compound from the dynamics of a Freedericks transition.

We also present the temperature dependence of the surface tension σ .

In the smectic A phase, we have been able to follow the beginning of the very rapid increase of η_1 below the transition ($10^{-2} < \Delta T < 3 \times 10^{-1} \text{ }^\circ\text{C}$), which leads to very large effective viscosity and anisotropy ($\eta_1/\eta_{\text{iso}} \sim 800$ for $\Delta T \sim 3 \times 10^{-1} \text{ }^\circ\text{C}$) and is a rather direct evidence for the existence of permeation.

2. Experimental set-up. — The viscosities η_1, η_2, η_3 have been deduced from velocity measurements of conventional Poiseuille flow in a well oriented nematic, in a way somewhat similar to Gähwiller's experiments [9]. The cell is shown schematically in figure 2 : the channel (thickness e , 1 mm width, 15 mm long) is

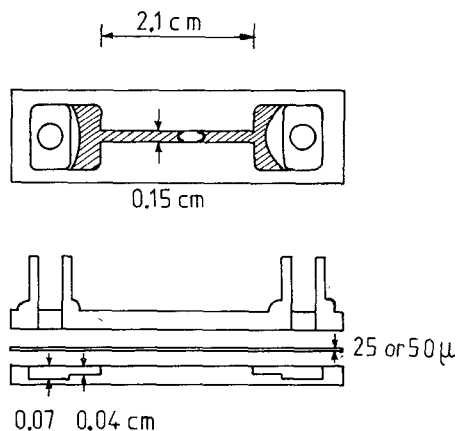


FIG. 2. — Top view and cross section of the cell showing the channel and the two lateral chambers. The liquid crystal remains in the thinnest part of the chambers by capillarity.

connected to two lateral chambers. This rather complicated geometry has been employed for several reasons :

— The chambers have a two steps profile (0.4 mm and 0.8 mm depth) and the liquid is stabilized in the central part of the cell by capillarity.

— The ratio of the channel to chamber cross section is about 150 for $e = 25 \text{ } \mu\text{m}$ and the displacement of the interface in the chamber is negligible during the experiment. For a $50 \text{ } \mu\text{m}$ thick channel, this is no longer valid, and we make use of this to deduce the surface tension term. We shall return to this point in paragraphe 3.

— The flow does not induce a gravitational pressure.

The cell is made from the assembly of a flat top cover having two nozzles, and a recessed bottom plate, which are stuck together by melting a plastic spacer. The exact geometrical characteristics of the channel are then measured with a microscope. The well defined orientation of the liquid crystal is obtained by previously treating the top and bottom parts of the cell in one of the following ways :

— By evaporation of a thin SiO layer under oblique incidence [10] for both planar orientations.

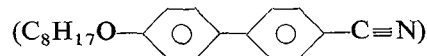
— By evaporation of a thin Au film under perpendicular incidence, and then coating with hexadecyl trimethyl-p-ammonium bromide for homeotropic orientation. A strong (30 V \rightarrow 70 V, 1000 Hz) voltage is applied between the semi transparent Au electrodes to prevent misorientation with the flow for that particular geometry (M 24 has a high positive dielectric anisotropy ~ 9).

The orientation and the absence of defects are continuously controlled during the experiment through a polarizing microscope. For geometries 1 and 3, for which no orienting fields are applied, we work with sufficiently low velocities to avoid misorientation : if a distortion is induced by the flow, it takes place over a distance [11].

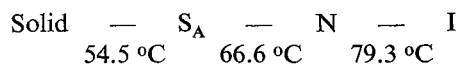
$$l = \left(\frac{K}{\eta v / e} \right)^{1/2}$$

(K is an elastic constant). The condition for unperturbed orientation is $l \sim e$. Typically, we maintain $\eta e v / K \lesssim 1$ for the two geometries.

The liquid crystal used is 4-n-octyloxy-4-cyano-biphenyl [12] (hereafter M 24)



which is successively



We have chosen this compound for several reasons :

— the nematic range is large : $T_{\text{NA}}/T_{\text{NI}} = 0.96$, and the transition enthalpy is in the range of 10^{-2} cal/g ⁽¹⁾, analog to the similar transition of

(1) Gray, G. W., Private communication.

cyanobenzilidene octyloxyanilin (CBOOA) [13], T_{NA} = smectic A-nematic, T_{NI} = nematic-isotropic transition temperature ;

— it was claimed to be a very stable liquid crystal.

We have determined the shift of the S_A -N transition temperature (determined optically) with time. It is very sample dependent, and we have not been able to determine the origin of the shift. Even working under inert atmosphere (argon) has resulted in a relatively weak stabilizing effect. In the most favourable case, the shift was not detectable over one experiment ($< 2 \times 10^{-3}$ °C for ~ 6 h), and smaller than 2×10^{-3} °C/h over a full month run. In other cases, it may be higher, and lies typically between 5 and 30×10^{-3} °C/h. This result seems rather disappointing, but one of the main advantages of octyloxy-cyanobiphenyl is the fact that it dissolves its impurities very well, and we have not been able to detect any T_c distribution in our samples, even after one month heating in contrast to CBOOA or butyloxybenzilidene octylanilin 40.8. This allows us to correct the transition temperature during an experiment, assuming a linear time dependence. This correction has been made, as an indicative test for some runs, and appears to be unimportant in the numerical results (2).

When filling the cell, a small air or argon bubble is introduced, which occupies the entire width of the channel, and serves as tracer. A small pressure difference ΔP is then applied between the two nozzles (typically 10 mm of water). This pressure difference is obtained through an air expander or through a small mechanical compression in a thermally insulated volume, and is measured with a two liquid manometer. When submitted to the pressure gradient, the liquid crystal flows, and the displacement d of the bubble — L. C. interface is observed optically with the microscope. A typical plot of d versus time t is shown in figure 3a, in the case of weak surface tension terms ($e = 23 \mu$). The plot is a straight line ; its slope determines the average velocity of the flow \bar{v} (3).

In the case of negligible surface tension effects from \bar{v} and Δp , we deduce :

$$\eta = A \frac{\Delta p}{\bar{v}} \quad (1)$$

(2) As can be seen on figure 6, which is a log plot of η_1 versus $T - T_{NA}$ the correction does not affect the slope of the curve : we work increasing the temperature from T_{NA} . The correction is small for the points located near T_{NA} , which are taken in a short time interval, and larger for the points far from T_{NA} , but that difference is compensated by the log log units.

(3) The presence of the bubble locally distorts the stream lines : they are parallel to x (Fig. 1) except in a boundary layer near the bubble, where they splay transversally, to compensate the velocity profile in the sample. The thickness of this layer is small compared to the length of the channel (typically 10^{-3}) and does not affect the viscosity measurement, except in the case of very high transverse viscosities.

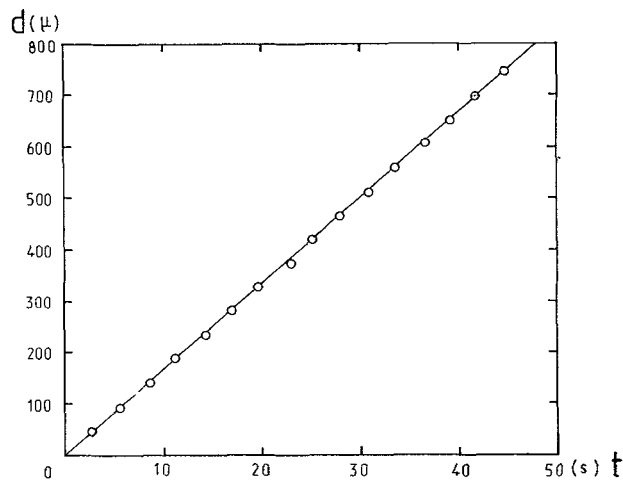


FIG. 3a. — Displacement d of the bubble versus time for a 23μ sample. $\Delta P = 12$ mm H_2O .

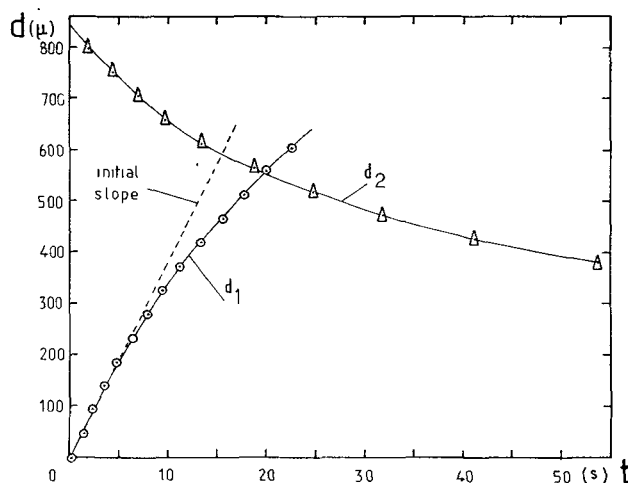


FIG. 3b. — For a 55μ sample, the displacement d of the bubble versus time is not linear due to surface tension effects. d_1 is the displacement with (forth) and d_2 without (back) pressure difference ($\Delta P = 12$ mm H_2O).

with

$$A = \frac{1}{12} \frac{e^2}{L} \quad (2)$$

for a parabolic profile. (L length of the channel minus length of the bubble). All the quantities in A are known, and we can have an absolute determination of η .

To follow the critical behaviour of the three viscosities near the S_A -N transition, the cell is placed in a double-stage oven. Each stage is a thick (1 cm) copper box, the temperature of which is electronically regulated through a platinum resistance sensor. The temperature of the outside stage is maintained 0.1 °C below the inside one. The temperature of the sample is deduced from another independent strain free platinum resistance, located just near the sample, with an accuracy of $\pm 2 \times 10^{-3}$ °C. The stability of the inner chamber temperature is better than 10^{-3} °C/h. Ther-

mal gradients over the sample have been determined, using very small differential thermocouples movable inside the channel. The most important source of thermal gradients is the light source of the microscope which introduces a hot point in the window area of the oven. Working with the minimum practicable lighting, the thermal gradients are kept smaller than 10^{-2} °C over the whole length of the channel.

The twist viscosity γ_1 has also been measured, using the dynamics of a planar to homeotropic Freedericksz transition as developed in reference [7]. An attenuated laser beam is sent through a 239 μ thick M 24 sample, inserted between two semi-transparent gold coated electrodes, in the same oven. The modulation of the transmitted intensity, between crossed polarizers, when the applied voltage is decreased from value larger than V_c to values smaller than V_c , is recorded and allows us to determine the time constant of the relaxation of the molecules, proportional to γ_1 .

3. Surface tension effects. — The detailed relation between v and ΔP is not always a straight line. In contrast to figure 3a (23 μ thick sample), we see experimentally that the $d(t)$ plot of figure 3b is no longer linear for a thick sample (55 μ , geometry 1). Moreover, if we remove the pressure gradient, the bubble/M 24 interface displaces in the opposite way, returning to some equilibrium position.

The first thing we can think of to explain this behaviour is that the two air/M 24 interfaces are to some extent pinned in the chambers, and that they distort when d increases, introducing some restoring force proportional to d and to the surface tension σ (the two air/M 24 interfaces in the chambers act like two opposite springs at the end of the channel). The motion of the bubble/M 24 interface is then given by :

$$v = \frac{A}{\eta} (\Delta p - \Delta p') \quad (3)$$

with

$$\Delta p' = \frac{2\sigma}{s} \frac{s}{S} d \quad (4)$$

where s and S are respectively the channel and chamber cross sections. In fact, this simple model has to be made slightly more complicated to take into account the following points :

i) The origin for d is some arbitrary point in the field of the microscope, and not necessarily the equilibrium position of the bubble, while the restoring pressure $\Delta p'$ has to be proportional to the distance from this equilibrium position. We have to write :

$$\Delta p' = \frac{2\sigma}{S} (d + b) \quad (5)$$

where $-b$ locates the equilibrium position of the bubble.

ii) The air/M 24 interfaces in the chambers are in fact not strongly anchored, and they drift slowly when

d increases. This diminishes the importance of the restoring forces, and by noting that b then depends on d ; to first order we can write,

$$b = b' - b'' d \quad 0 < b'' < 1$$

($b'' = 0$ corresponds to a perfectly anchored interface, and $b'' = 1$ to a perfectly free interface) and $\Delta p'$ becomes

$$\Delta p' = \frac{2\sigma}{S} (1 - b'') d + \frac{2\sigma}{S} b' \quad (6)$$

iii) Some additional constant term has to be added. $-\Delta p'' = \pm a$. We interpret it as a friction term, introduced by the bubble, because it changes sign with the direction of the displacement d .

Finally, the equation of motion is :

$$v_1 = \frac{A}{\eta} \left[\Delta p - \left(a + \frac{2\sigma}{S} b' \right) - \frac{2\sigma}{S} (1 - b'') d \right] \quad (7)$$

$$v_2 = \frac{A}{\eta} \left[a - \frac{2\sigma}{S} b' - \frac{2\sigma}{S} (1 - b'') d \right] \quad (8)$$

(the subscripts 1 and 2 denote the presence or absence of an external pressure gradient).

The solutions of (7) and (8) are respectively

$$d_1 = d_M (1 - e^{-\alpha_1 t_1}) \quad (9)$$

with

$$d_M = \frac{S}{2\sigma} (\Delta p - a) - b' \quad (10)$$

$$\alpha_1 = \frac{2A\sigma}{\eta S} (1 - b'') \quad (11)$$

($t_1 = 0$ for $d_1 = 0$)

$$d_2 = (d_0 - C) e^{-\alpha_2 t_2} + C \quad (12)$$

with

$$C = \frac{aS}{2\sigma} - b' \quad (13)$$

$$\alpha_2 = \frac{2A\sigma}{\eta S} \quad (14)$$

d_0 is the position of the bubble interface when the pressure gradient is taken off ($t_2 = 0$ for $d_2 = d_0$, the maximum elongation). Notice that in the case of zero pressure gradient, the stress on the air/M 24 interface is smaller, and b'' is negligible.

As can be shown on figure 4, eq. (9) and (12) will describe the shape of the $d(t)$ curves of figure 3b.

At this stage, several remarks have to be made :

i) α_1 and α_2 are proportional to A , which is strongly dependent on thickness ($A \propto e^2$). For this reason, $d(t)$ seems linear for a 25 μ channel (Fig. 3a). The surface tension terms are only visible for the 50 μ thick samples.

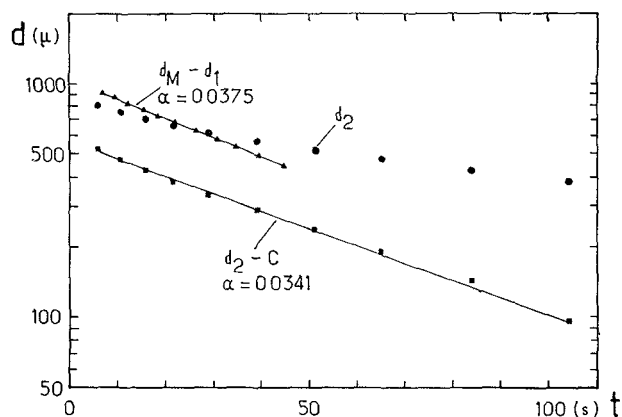


FIG. 4. — Displacement of the bubble forwards (d_1) and backwards (d_2) versus time. For the meaning of d_M , C and α , see text. α is the logarithmic decrement in s^{-1} .

ii) α_1 and α_2 are inversely proportional to η : for the 50 μm thick channels, the surface tension terms are much more visible in geometry 1 than in the two other geometries where the viscosities are two or three times larger.

iii) The initial slope of the $d(t)$ curve is

$$v_1(0) = \frac{A}{\eta} \left(\Delta p - \left(a + \frac{2\sigma}{S} b' \right) \right). \quad (15)$$

It depends linearly on Δp . From the slope of the $v_1(0)$ versus Δp curve, we can deduce η (A only contains geometrical factors). The accuracy for absolute η measurements is about 25%; the uncertainty is due principally to the sample thickness e , which is only known to a few microns, and to the fact that the correcting terms a and b' are not well determined. For relative values of η , the accuracy is much better (typically < 10%) especially in the case of 25 μm samples: we have seen that α_1 is then smaller by a factor of 4 ($A \sim e^2$). As we work with almost the same velocities, we then use a pressure gradient four times larger than in the case of 50 μm samples, and the correcting terms $a + \frac{2\sigma}{S} b'$ are negligible.

The method has been checked with a standard liquid (oleic acid) at different temperatures, and the agreement with both absolute value at 25 $^\circ C$ and the activation energy from the literature is correct (25.2 cPo and 0.31 eV measured, compared to 29.35 cPo and 0.26 eV [14]).

An independent measurement with a cone-plate viscometer on the same M 24 in the isotropic phase has given 8.1 cPo at $T = 85^\circ C$ in good agreement with our absolute determination of 7.8 cPo.

We can now return to figure 4: we have plotted $\log d_2$ versus t , and $\log (d_2 - C)$ versus t , where C is adjusted to obtain the best fit. We see that our results

agree well with eq. (12) and from the slope α_2 of the $\log (d_2 - C)$ versus t straight line, we can extract (eq. (14))

$$\sigma = \frac{\alpha_2 \eta S}{2A}.$$

The experimental values of $\sigma(t)$ are plotted in figure 5, using the values of η_1 determined as explained

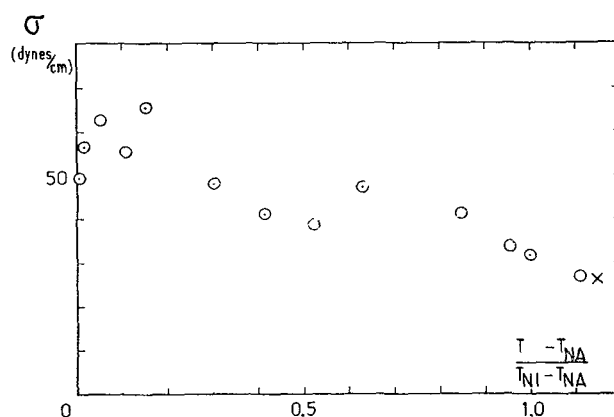


FIG. 5. — Surface tension versus the reduced temperature: \odot from the $d_2 - C$ curves, \times from the drop weight method.

above, and which are discussed in paragraph 4. They are in good agreement with other values: light scattering by surface waves [15], or measurement by the drop weight method in the isotropic phase, which has given 26.2 dynes/cm at 80 $^\circ C$. In figure 4, $\log (d_M - d_1)$ is also plotted, where d_M is adjusted to obtain a straight line (eq. (9)). The difference between the slopes α_1 and α_2 is a measure of the importance of drift of the interfaces in the chambers, characterized by b'' . This term is strongly sample dependent, and depends in fact on the state of the glass surfaces in the chambers.

In conclusion, for geometry 1, the accuracy of the η_1 measurements is larger with a 25 μm thick channel than with a 50 μm one, but the case of the 50 μm channel allows us to determine the air/M 24 surface tension σ . For the two other geometries, both thick and thin samples can be used, to deduce the viscosities with comparable accuracy.

4. Behaviour of the viscosities in the nematic range. —

In figure 6, the viscosities η_1, η_2, η_3 , corresponding to molecules respectively parallel to x, z and y , are plotted versus temperature. The interesting part of the diagram is located near T_{NA} : η_2 and η_3 have a non singular behaviour, while η_1 strongly diverges for $T \sim T_{NA}$. Figure 7 gives the variation of η_1 versus $T - T_{NA}$ in log log units. T_{NA} has been taken as the very well defined knee existing in the $\eta(T)$ curve. It is very near ($\sim 10^{-2}^\circ C$ above) the optically determined T_{NA} and the difference is of the order of the thermal gradients in the channel, with the right sign. A linear behaviour is observed in the whole nematic

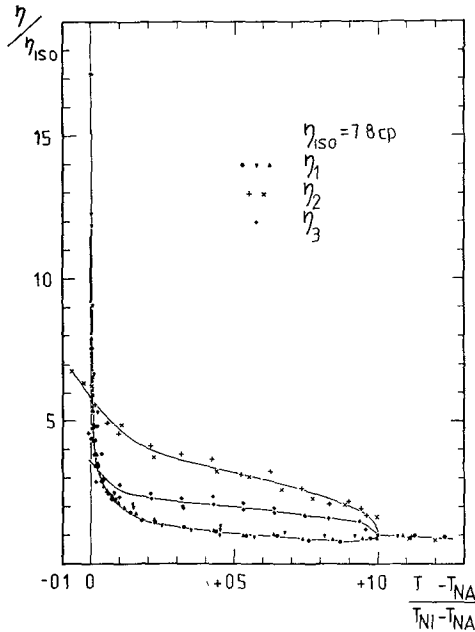


FIG. 6. — Variation of the three viscosities η_1, η_2, η_3 versus the reduced temperature. The η_1 values for $T < T_{NA}$ fall outside the figure and are plotted in figure 7.

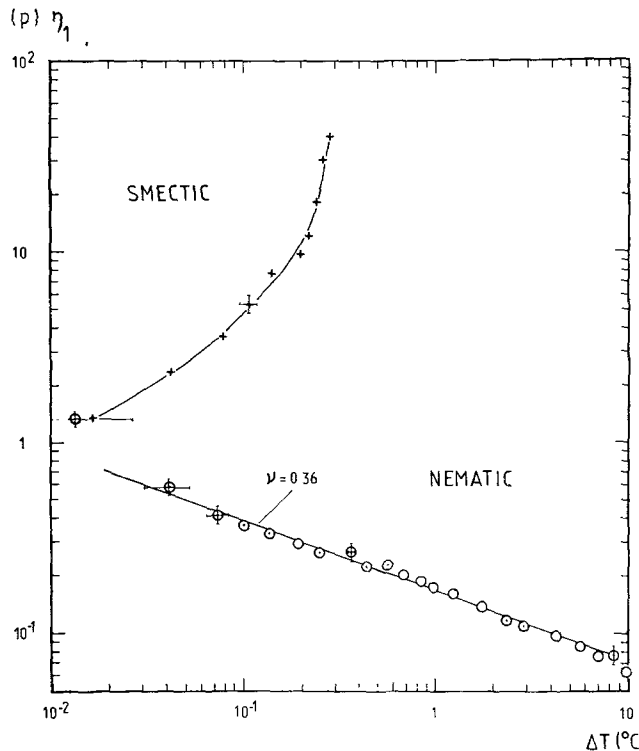


FIG. 7. — η_1 versus temperature follows a law in $\Delta T^{-\nu}$ with $\nu = 0.36$ in almost all the nematic range. η_1 is also given in the smectic range in the permeation regime.

range, except very close to the isotropic transition. The slope of the straight line is 0.36 ± 0.05 in good agreement with the Helium analogue prediction [3, 4] and significantly different from 0.5.

A least square fit with a five parameter law

$$\frac{\eta_1}{\eta_{iso}} = \mathcal{A} e^{W/kT} + \mathcal{B}(T - T_{NA})^{-\nu} \quad (16)$$

gives

$$\begin{aligned} \mathcal{A} &= 0.651 \times 10^{-6} \\ W &= 1.788 \times 10^{-14} \text{ erg} \\ \mathcal{B} &= 2.106 \\ T_{NA} &= 66.661 \text{ }^\circ\text{C} \text{ (}^4\text{)} \\ \nu &= -0.364. \end{aligned}$$

η_{iso} is the measured viscosity in the isotropic phase close to T_{NI} .

The first regular term of eq. (16) corresponding to the best fit, $\mathcal{A} e^{W/kT} \times \eta_{iso} \simeq 7.4 \times 10^{-8} \text{ P}_0$ at T_{NI} , is indeed a very small viscosity for a nematic and similarly for W . But those values are not very confident: the regular term is almost negligible in front of the divergent term even far from T_{NA} ($\sim 7.4 \times 10^{-8}$ compared to 0.078 P_0 at $T \sim T_{NI}$) and thus badly determined by the fit. A variation of \mathcal{A} and W over a large range ($10^{-2} \text{ eV} < W < 0.4 \text{ eV}$, and correlatively $0.25 \times 10^{-6} < \mathcal{A} < 0.65 \times 10^{-6}$), does not affect sensitively the quality of the fit, the critical exponent remains between -0.36 and -0.38 .

Moreover :

i) If we take as plausible background the value of η_1 keeping the same anisotropy as in a standard nematic like MBBA (ratio $\eta_2/\eta_1 \sim 4$), one still obtains a linear behaviour of η_1 in log log units but over two decades only. The corresponding exponent 0.41 remains in the experimental errors.

ii) It is never possible to find a background term in $\mathcal{A} e^{W/kT}$ which allows to fit the experimental points with a 0.5 power law over the entire range of temperature.

The η_1 measurements have been reproduced with five different samples and are all compatible with an exponent :

$$\nu = 0.36 \pm 0.05$$

as determined over three decades of temperature. $\gamma_1(T)$ is plotted in figure 8 and also exhibits a divergence near T_{NA} . Figure 9 gives $\gamma_1(T)$ in log log units, and we see that the determination of a critical exponent is much more delicate than in the case of η_1 , as it is not so clearly linear. For γ_1 , we expect a temperature dependence

$$\gamma_1 = \mathcal{C} S^2 e^{+\varepsilon S/kT} + \mathcal{B}(T - T_c)^{-\nu} \quad (17)$$

\mathcal{C} and ε are constants, S is the nematic order parameter and \mathcal{B} and ν have the same values than in (16). The regular term $\mathcal{A} e^{W/kT}$ of (16) being negligible, the difference $\gamma_1 - \eta_1$ gives the regular term of γ_1 , which is shown in figure 8 (dotted line). This regular term is an

(4) The value of T_{NA} extracted from the fit is very close to the temperature at which a knee is observed in the $\eta_1(T)$ curve, and if a T^* exists, the difference $T_{NA} - T^*$ is smaller than $10^{-2} \text{ }^\circ\text{C}$.

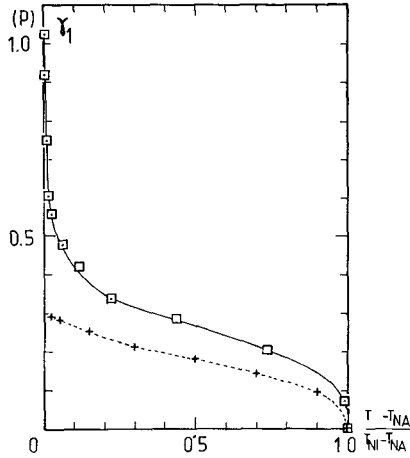


FIG. 8. — \square twist viscosity γ_1 versus the reduced temperature ; $+$ variation of the regular part of γ_1 as deduced from η_1 measurements.

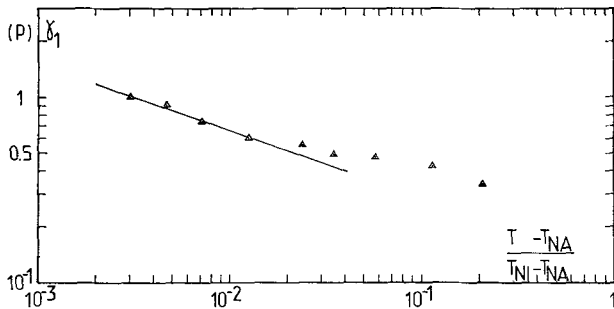


FIG. 9. — Variation of the twist viscosity γ_1 versus the reduced temperature in log log units. The slope gives $\nu \simeq 0.37$.

important fraction of the total viscosity and it is delicate to make the appropriate correction. The only thing we can say is that our $\gamma_1(T)$ measurements are not incompatible with a critical exponent of 0.36, but one more decade in ΔT should certainly be necessary to deduce any critical exponent from $\gamma_1(T)$.

From the different $\eta_1, \eta_2, \eta_3, \gamma_1$ viscosities, we can deduce four of the five Leslie friction coefficients, as

$$\eta_1 = \alpha_3 + \frac{\alpha_2 + \alpha_4 + \alpha_5}{2} \quad (18)$$

$$\eta_2 = \frac{-\alpha_2 + \alpha_4 + \alpha_5}{2} \quad (19)$$

$$\eta_3 = \frac{\alpha_4}{2} \quad (20)$$

$$\gamma_1 = \alpha_3 - \alpha_2. \quad (21)$$

The corresponding values are plotted versus temperature in figure 10.

An important result of those experiments has been to reveal that the amplitude of the divergent term is very large. The order of magnitude of β is 100 times larger than the first prediction by Brochard and Jähmig [4a] and actually in agreement with the recent evaluation of Brochard which takes into account the overdamping of the second sound in the smectic phase [4b].

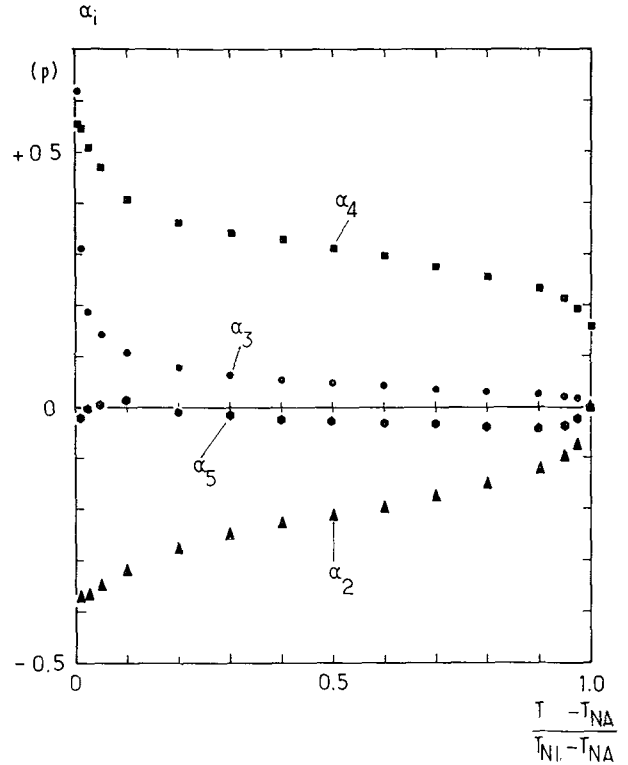


FIG. 10. — Variation of the Leslie coefficients α_i versus reduced temperature.

5. Viscosities in the smectic A phase. — We have measured the mean velocity for the geometries 1 and 2 (molecules respectively parallel to x and z), in a narrow temperature range close to T_{NA} ($10^{-2} \text{ }^\circ\text{C} < T_{NA} - T < 3 \times 10^{-1} \text{ }^\circ\text{C}$). The behaviour of the effective viscosity

$$\eta_{1\text{eff}} = \frac{1}{12} \frac{e^2}{L} \frac{\Delta p}{\bar{v}}$$

is shown on the log log plot of figure 7 : it increases very rapidly with decreasing temperatures, and for $T_{NA} - T > 3 \times 10^{-1} \text{ }^\circ\text{C}$, the system becomes completely rigid : no flow can be observed even over one day, for $\Delta p = 12 \text{ mm H}_2\text{O}$. By increasing the pressure difference, no flow is observed, for $\Delta T > 2 \times 10^{-1} \text{ }^\circ\text{C}$, up to a threshold value of Δp , for which the smectic layers break down somewhere in the sample, forming some small focal conics which allow flow, by rolling over one another. The stream lines then take up a complicated shape, crossing the smectic layers only in the places where the focal conics have formed, as shown in figure 11.

The shape of the $\log \eta_1$ versus ΔT curve can be qualitatively explained in the following terms : in a purely permeation regime of flow, the velocity profile is flat, with a mean velocity $\bar{v} = -\lambda p \Delta p$ (λp is the permeation constant) except in two small boundary layers of size $\kappa^{-1} = (\lambda p \eta_1)^{1/2}$. Close to the smectic A nematic transition, η_1 is expected to diverge in a way

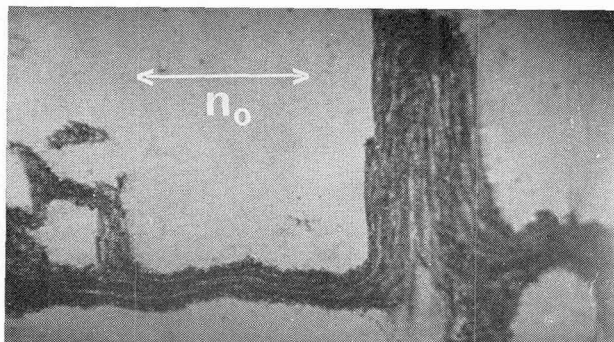


FIG. 11. — Zig zag stream lines visualised by chains of focal conics : the smectic layers break down under a pressure difference larger than a threshold value a few degrees below T_{NA} for geometry 1 ($\nabla P \parallel n_0$).

which is symmetric with what happens in the nematic region, i. e. as $(T_{NA} - T)^{-0.33}$ while λp is expected to diverge as $(T_{NA} - T)^{-1}$ [3] and the size of the boundary layer diverges as $(T_{NA} - T)^{-0.66}$. Taking

$$\lambda_p = \frac{d^2}{\eta_0} \left(\frac{\Delta T}{T} \right)^{-1}$$

(d is the thickness of the smectic layers and η_0 a regular viscosity far from T_{NA}) and

$$\eta = \eta_0 \left(\frac{\Delta T}{T} \right)^{-0.33} \quad [4b],$$

we obtain as an estimation of

$$\kappa^{-1} \sim d \left(\frac{\Delta T}{T} \right)^{-0.66}, \quad \text{i. e. } 3 \mu \text{ for } \Delta T = 10^{-2} \text{ } ^\circ\text{C}.$$

This boundary layer is then not negligible relative to the channel thickness, and the velocity profile is given [16] by

$$v(z) = -\lambda_p \nabla p \left(1 - \frac{\text{Ch } \kappa z}{\text{Ch } \kappa \frac{e}{2}} \right). \quad (22)$$

The mean velocity is

$$\bar{v} = \frac{1}{e} \int_{-e/2}^{e/2} v(z) dz = -\lambda_p \nabla p \left(1 - \frac{\text{th } \kappa \frac{e}{2}}{\kappa \frac{e}{2}} \right). \quad (23)$$

The effective viscosity is thus expected :

- i) to diverge very close to T_{NA} , as $(T_{NA} - T)^{-0.33}$,
- ii) to vary as $1/\lambda p \sim T_{NA} - T$ when ΔT increases,
- iii) for larger ΔT , the temperature dependence of λp^{-1} may involve larger powers of ΔT as it certainly contains an activation energy.

From the upper part of figure 7, we see that we pass progressively from a regime of non negligible boundary layers (slope smaller than 1) to a true permeation regime (slope 1, and larger than 1 for $\Delta T > 10^{-1}$ $^\circ\text{C}$).

We do not work with small enough ΔT to observe the divergence of $\eta_{1\text{eff}}$.

The behaviour of η_2 is shown on the left part of figure 6, and is completely different from the case of $\eta_{1\text{eff}}$: an increase is observed, which is always followed by buckling instabilities of the layers [17], nucleated by the flow (the molecules tend to tilt in the direction of the flow, even if a high (70 V) stabilizing voltage is applied to the sample).

For the third geometry (molecules parallel to y) we have not been able to deduce η_3 : for that geometry, the transverse component of the flow, near the bubble corresponds to the very high $\eta_{1\text{eff}}$ viscosity, and is no longer negligible. The size of the boundary layer near the bubble (where the stream lines are no longer parallel to x) can easily be seen by following the motion of dust particles : it increases progressively when the temperature is decreased, while the flow is reduced, leading to an apparent increase in η_3 .

However, the remarkable feature of the smectic phase is the really enormous anisotropy of viscosities : typically for

$$T_{NA} - T = 3 \times 10^{-1} \text{ } ^\circ\text{C}, \quad \frac{\eta_{1\text{eff}}}{\eta_2} = 144.$$

6. Conclusion. — We have measured four viscosities η_1, η_2, η_3 and γ_1 in the nematic range of M 24. Close to the nematic smectic A phase transition η_2 and η_3 are regular while η_1 and γ_1 exhibit an important divergence. The η_1 behaviour may be characterized by a critical exponent $\nu = 0.36 \pm 0.05$, not very sensitive to the exact value of the background term which remains always small in front of the divergent part. The M 24 behaviour seems to agree rather well with the helium analog prediction and the magnitude of the divergent term is well described by the last theoretical considerations based upon a dimensional argument. However, the experimental accuracy is not sufficient to exclude the existence of successive exponent regimes.

In the smectic A phase of M 24, we have measured the two viscosities η_1 and η_2 , corresponding to a flow respectively normal or parallel to the smectic layers. The observed anisotropy η_1/η_2 is enormous, and of the order of 150 for $T_{NA} - T \simeq 0.3$ $^\circ\text{C}$. This is at the onset of permeation, in a regime where the boundary layers are not negligible. For larger values of the permeation constant ($T_{NA} - T > 3 \times 10^{-1}$ $^\circ\text{C}$) the layers prefer to break down and to adopt the shape of focal conics which help the flow by rolling over one another. Experiments with more rigid smectic A are now in progress to find evidence for the characteristic « bouchon » profile of a true permeation regime.

Acknowledgements. — We are grateful to M. Bourgain of the Biophysics and Biomathematics Lab, CHU La Salpêtrière, Paris, for the cone-plate measurements of viscosity and to D. Taupin for the numerical fitting. We want to acknowledge F. Brochard for many fruitful discussions.

References

- [1] McMILLAN, W. L., *Phys. Rev. A* **6** (1972) 936.
McMILLAN, W. L., *Phys. Rev. A* **9** (1974) 1720.
- [2] DE GENNES, P. G., *Solid State Commun.* **10** (1972) 753.
- [3] BROCHARD, F., *J. Physique* **34** (1973) 411.
- [4a] JÄHNIG, F., BROCHARD, F., *J. Physique* **35** (1974) 301.
- [4b] BROCHARD, F., *J. Physique Colloq.* **37** (1976) C3-85.
- [5] HALPERIN, B. I., LUBENSKY, T. C., MA, S. K., *Phys. Rev. Lett.* **32** (1974) 292.
- [6] HARDOUIN, F., ACHARD, M. F., GASPAROUX, H., *Solid State Commun.* **14** (1974) 453.
GASPAROUX, H., HARDOUIN, F., ACHARD, M. F., SIGAUD, G., *J. Physique Colloq.* **36** (1975) C 1-107.
HUANG, C. C., PINDAK, R. S., FLANDERS, P. J. and HO, J. T., *Phys. Rev. Lett.* **33** (1974) 400.
WISE, R. A., OLAH, A. and DOANE, J. W., *J. Physique Colloq.* **36** (1975) C 1-117.
BACRI, J. C., *J. Physique Colloq.* **36** (1975) C 1-123.
LANGEVIN, D., *J. Physique Colloq.* **36** (1975) 745.
- [7] D'HUMIÈRES, D., LÉGER, L., *J. Physique Colloq.* **36** (1975) C 1-113.
- [8] CHU, K. C., McMILLAN, W. L., *Phys. Rev. A* **11** (1975) 1059.
- [9] GÄHWILLER, C. H., *Mol. Cryst. Liq. Cryst.* **20** (1973) 301.
- [10] JANNING, J. L., *Appl. Phys. Lett.* **21** (1972) 173.
URBACH, W., BOIX, M. and GUYON, E., *Appl. Phys. Lett.* **25** (1974) 479.
- [11] DE GENNES, P. G., *The Physics of Liquid Crystals* (Clarendon Press) 1974, p. 171.
- [12] GRAY, G. W., HARRISON, K. J., NASH, J. A., CONSTANT, J., HULME, D. S., KIRTON, J., RAYNES, E. P., Proc. Symposium Ordered Fluids & Liquid Crystals, Chicago, Aug. 1973.
- [13] DJUREK, D., BATURIC-RUBCIC, J., FRANULOVIC, K., *Phys. Rev. Lett.* **33** (1974) 1126.
- [14] VAN VELZEN, D., LOPES CARDOZO, R., LANGENKAMP, H., Euratom report n° EUR 4735e (1972) Ispra Establishment (Italy).
- [15] LANGEVIN, D., to be published.
- [16] DE GENNES, P. G., *Phys. Fluids* **17** (1974) 1645.
- [17] RIBOTTA, R., Thèse Orsay (1975).